HHS Public Access

Author manuscript

Neuron. Author manuscript; available in PMC 2024 March 15.

Published in final edited form as:

Neuron. 2023 March 15; 111(6): 797–806.e6. doi:10.1016/j.neuron.2022.12.027.

Dorsomedial Prefrontal Hypoexcitability Underlies Lost Empathy in Frontotemporal Dementia

Hannah L. Phillips[1,2], **Huihui Dai**[1], **So Yoen Choi**[3], **Karen Jansen-West**[5], **Alexis S. Zajicek**[1,2], **Luke Daly**[3,4], **Leonard Petrucelli**[5], **Fen-Biao Gao**[3,4], **Wei-Dong Yao**[1,2,6,7,*]

[1]Department of Psychiatry and Behavioral Sciences, State University of New York Upstate Medical University, Syracuse, NY 13210, USA.

[2]Neuroscience Graduate Program, State University of New York Upstate Medical University, Syracuse, NY 13210, USA.

[3]Department of Neurology, University of Massachusetts Chan Medical School, Worcester, MA 01655, USA.

[4]Neuroscience Program, University of Massachusetts Chan Medical School, Worcester, MA 01655, USA.

[5]Department of Neuroscience, Mayo Clinic, Jacksonville, FL 32224, USA.

[6]Department of Neuroscience and Physiology, State University of New York Upstate Medical University, Syracuse, NY 13210, USA.

SUMMARY

Empathic function is essential for the well-being of social species. Empathy loss is associated with various brain disorders and represents arguably the most distressing feature of frontotemporal dementia (FTD), a leading form of presenile dementia. The neural mechanisms are unknown. We established an FTD mouse model deficient in empathy and observed that aged somatic transgenic mice expressing GGGGCC repeat expansions in *C9orf72*, a common genetic cause of FTD, exhibited blunted affect-sharing and failed to console distressed conspecifics by affiliative contact. Distress-induced consoling behavior activated the dorsomedial prefrontal cortex (dmPFC), which developed profound pyramidal neuron hypoexcitability in aged mutant mice. Optogenetic dmPFC inhibition attenuated affect-sharing and other-directed consolation in wildtype mice, whereas chemogenetically enhancing dmPFC excitability rescued empathy deficits in mutant mice, even

*Correspondence: yaow@upstate.edu (W.-D.Y.).

[7]Lead contact.

Author contributions: Conceptualization and Methodology, H.L.P. and W.-D.Y.; Investigation, H.L.P., H.D., S.Y.C., K.J.-W., A.S.Z., and L.D; Formal Analysis, H.L.P., S.Y.C., L.D. and W.-D.Y.; Writing - Original Draft, H.L.P. and W.-D.Y.; Writing - Review & Editing, H.L.P., L.P., F.-B.G. and W.-D.Y.; Resources, L.P. and F.-B.G.; Funding Acquisition, H.L.P., L.P., F.-B.G. and W.-D.Y.; Supervision, L.P, F.-B.G. and W.-D.Y.

Inclusion and Diversity: We support inclusive, diverse and equitable conduct of research.

Declaration of interests: F.-B. G. has an active research agreement with and receives funding from Stealth BioTherapeutics. The other authors declare no competing interests.

at advanced ages when substantial cortical atrophy had occurred. These results establish cortical hypoexcitability as a pathophysiological basis of empathy loss in FTD and suggest a therapeutic strategy.

In Brief:

Lost empathy is a defining clinic presentation of FTD. Phillips et al. develops an FTD mouse model that exhibits blunted affect-sharing and incapacity to comfort distressed partners due to decreased neuronal excitability in the dmPFC. Enhancing dmPFC activity restores empathy in aged mutant mice, even when substantial neurodegeneration had occurred.

Graphical Abstract

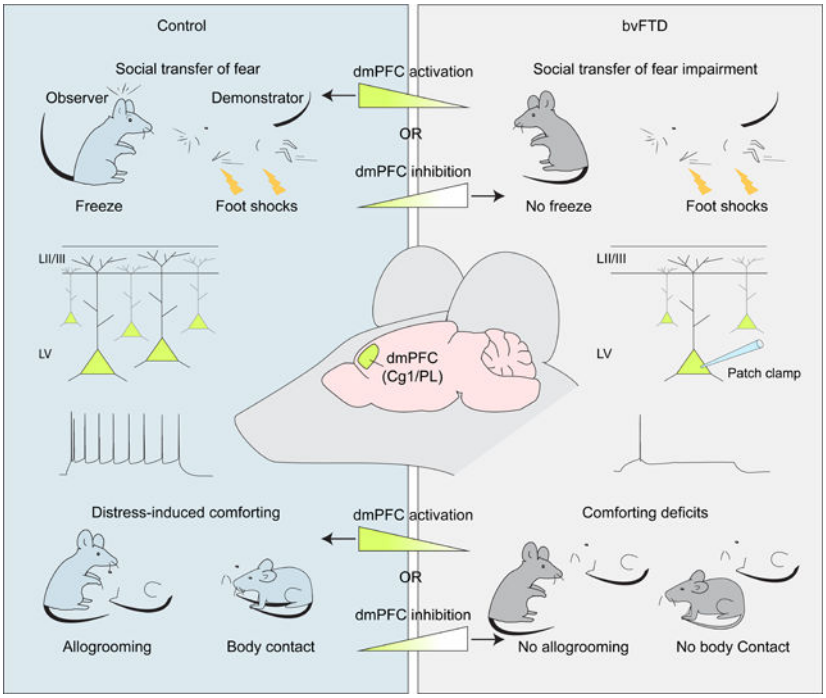

Keywords

Frontotemporal dementia; empathy; C9orf72; dorsomedial prefrontal cortex; hypoexcitability

INTRODUCTION

Empathy, the capacity to understand and share the affective states of another and respond appropriately, plays fundamental roles in one's well-being, kinship, and social life[1]. While common in humans and some nonhuman species[1], empathy, or its evolutionarily conserved forms with varying levels of self-other recognitions and affective-cognitive complexities, is observed across diverse social species, including rodents[2,3]. Rodents exhibit behavioral homologs of human empathy and empathetically motivated prosocial behaviors, including social transfer of fear or pain and emotional contagion[4–8], consolation toward distressed partners[7,9], and helping and sharing [10]. The anterior (ACC) and medial

cingulate (MCC) cortices, central nodes encoding information about affective states of others[11,12], along with regions in distributed affective and cognitive neural networks, e.g. the medial prefrontal cortex (mPFC), mediate human empathy[13,14]. In mice, the ACC and its descending pathways regulate social transfer of affect in a circuit- and valence-dependent manner[5,8,15–17]. However, the neural mechanisms of empathy remain largely undefined. In addition, abnormalities in empathy manifest in various psychiatric and neurological diseases[18,19], but the neurophysiological basis of empathy impairments remains unknown for any disease.

Frontotemporal dementia (FTD) is a leading form of presenile dementia associated with focal but progressive degeneration of frontal and/or temporal lobes and encompasses a spectrum of clinical syndromes[20,21]. About half of all FTD cases are behavioral variant FTD (bvFTD) characterized by marked changes in personality, judgement, inhibitory control and affect, including loss of empathy, arguably the most distressing condition for family and caretakers[20–22]. While most FTD occurs sporadically, a significant fraction of cases (~40–50%) are linked to mutations of over a dozen genes with diverse molecular and cellular functions[23]. A GGGGCC (G_4C_2) hexanucleotide repeat expansion in the chromosome 9 open reading frame 72 (*C9orf72*) gene is the most common genetic cause of both bvFTD (c9FTD) and amyotrophic lateral sclerosis (c9ALS)[24,25], a motoneuron degeneration disease that overlaps with FTD clinically and pathologically[23,26]. Strikingly, despite the molecular and genetic heterogeneity of bvFTD, behavioral impairments, lost empathy in particular, remain a common and defining feature suggesting that fundamental neurophysiological mechanisms at the cellular and circuit levels are at play. However, such mechanisms are largely unknown.

RESULTS

Other-directed consolation and emotional contagion in mice

We first set out to develop a mouse paradigm (Figure 1) that captures both emotional contagion, a basic form of affective empathy, and distress-induced, other-directed consolation, an empathy-driven prosocial behavior initially observed in the rodent species prairie vole[7]. A naive test mouse (observer) and a same-sex, unrelated, non-familiar conspecific (demonstrator) were allowed to freely interact in a home-cage interaction session (HC1), followed by an observational fear conditioning (OFC) session where the demonstrator received repetitive foot-shocks with the observer watching and concluded by a second home-cage session (HC2) where the two mice were reunited (Figure 1A). During HC1, observer mice exhibited characteristic behavioral repertoires including social investigative (head, body, and anogenital sniffing) and non-social (rearing, self-grooming, locomotion and inactive) behaviors (Figure 1B). During HC2 reunion following OFC, however, observers also displayed robust prosocial allogrooming and, more predominately, body contact (brief but repeated body-touching or prolonged body-huddling) toward distressed demonstrators (Figure 1B and 1C and Video S1). These other-directed affiliative behaviors were nearly exclusively seen in observers interacting with shocked, but not non-shocked demonstrators, and during HC2, but not HC1, with significantly longer duration, larger numbers of bouts, and shorter onset latency (Figure 1D–1H, Figure S1A and S1B

and Video S1). Importantly, demonstrators did not exhibit allogrooming toward observers (Figure S1C), and instead showed a marked increase in self-grooming (Figure 1I) and immobility as well as decreased number of social approaches in HC2 (Figure S1D and S1E), signaling an elevated state of distress. Thus, the other-directed affiliative behaviors are specific to and initiated by the observers in response to demonstrators in distress. As expected, observer mice showed a significant increase of observational fear during both OFC and retrieval 24 hours later (Figure 1J and 1K), as well as a modest but significant increase in self-grooming in HC2 (Figure 1I), suggesting emotional contagion.

A purported benefit of other-oriented prosocial behaviors is comforting[27]. To test whether other-directed affiliative behavior by observers had a stress-relieving effect on demonstrators, we examined the anxiety level of distressed demonstrators following isolation or reunion with observers in HC2 (Figure 1L). In an open field, demonstrators that were alone during HC2 showed a significant decrease in center-to-total distance ratio post-shock compared to baseline, indicating an increase in anxiety (Figure 1M). In contrast, demonstrators that were reunited with observers during HC2 did not exhibit an increase in anxiety (Figure 1M), suggesting a calming effect provided by the observer to the demonstrator, consistent with social buffering of stress previously shown in rodents[7,9]. Together, we have established a behavioral paradigm that captures both distress-induced affiliative (DIA) consolation behavior and affect-sharing emotional contagion in mice.

Empathic deficits in aged $(G_4C_2)_{66}$/EGFP mice

Mouse models of empathy loss associated with FTD were envisioned[28], but have yet to become available. To establish such a model, we adopted an adeno-associated virus (AAV)-induced somatic transgenic mouse strain that expresses 66-G_4C_2 hexanucleotide repeat expansions throughout their CNS and develop characteristic c9FTD pathologies[29,30]. Mice at postnatal day 0 (p0) received intracerebroventricular (ICV) microinjections of AAV9 expressing $(G_4C_2)_{66}$ and EGFP ($(G_4C_2)_{66}$/EGFP), $(G_4C_2)_2$ and EGFP ($(G_4C_2)_2$/EGFP) or EGFP alone, with EGFP serving as a control while labelling infected neurons (Figure S2A and S2C). At ~12 months, an age equivalent to 45–50 human years when most FTD symptoms peak[31], $(G_4C_2)_{66}$/EGFP mice displayed 22–25% neuron loss in the mPFC relative to control $(G_4C_2)_2$/EGFP and EGFP mice (Figure S2B), indicating substantial prefrontal atrophy. Consistent with previous reports[29,30], $(G_4C_2)_{66}$/EGFP mice showed characteristic poly(GR) and poly(GA) dipeptide repeat (DPR) protein inclusions in EGFP-positive neurons in the mPFC (Figure S2C).

When tested in the DIA assay, aged $(G_4C_2)_{66}$/EGFP observers showed marked loss of affiliative allogrooming and body contact toward distressed demonstrators in HC2 (Figure 2A), with significantly shorter duration, lower bout number, and longer latency of other-directed affiliation compared to age-matched $(G_4C_2)_2$/EGFP and EGFP observers (Figure 2B–2D and Video S1). Aged $(G_4C_2)_{66}$/EGFP observers also exhibited significantly less observational fear during both OFC (Figure 2F) and 24-hour retrieval (Figure 2G), as well as blunted distress-induced self-grooming (Figure 2E), suggesting impaired emotional contagion. General self-grooming capacity, however, was intact in mutant mice (Figure S2G). The empathic deficits in $(G_4C_2)_{66}$/EGFP mice were unlikely due to potential deficits

in olfactory functions, which are involved in both vicarious fear and allogrooming in mice[5,9], as mutant mice showed similar levels of olfactory sensitivity and discrimination relative to controls (Figure S2H and S2I).

The lack of other-directed affiliative behaviors of $(G_4C_2)_{66}$/EGFP mice in HC2 was unlikely due to their inability to acquire vicarious fear in OFC, because mutant observers still showed significantly less affiliative behaviors than EGFP mice when demonstrators received shocks without their direct observation in a non-observational DIA assay (Figure 2H and 2I and Figure S2J–S2L). These mice, as expected, showed impaired distress-induced self-grooming in HC2 (Figure S2M), consistent with an emotional contagion deficit. Finally, in both observational and non-observational DIA paradigms, mutant mice spent more time locomoting in HC2, likely a result of reduced affiliative drive, but were not significantly or consistently affected in other non-social behaviors (Figure 2E and Figure S2D–S2F, S2N–S2P), suggesting little contributions of these behaviors to empathy deficits in mutant mice.

dmPFC hypoexcitability in aged $(G_4C_2)_{66}$/EGFP mice

We next explored the potential mechanism underlying the lost empathy in mutant mice. Because the prefrontal underpinnings of consolation in mice have not been determined, we first identified the PFC subregions activated in observer mice during our observational DIA test using c-Fos (an immediate early gene protein) activity mapping. Significantly more c-Fos-positive cells were detected in cingulate area 1 (Cg1) and prelimbic cortex (PL), referred to as dmPFC, in observers exposed to shocked demonstrators, compared with non-shocked controls (Figure 3A–3C). The dmPFC regulates high-order social behaviors[32–35] and represents a viable candidate for prosocial consolation behavior.

We then investigated the intrinsic excitability of dmPFC layer V (LV) pyramidal neurons, the major output neurons projecting to downstream structures[36] to regulate behaviors. Using slice electrophysiology (Figure 3D), we found that the amount of current required to evoke the first action potentials (APs) in $(G_4C_2)_{66}$/EGFP-expressing neurons was strikingly increased compared to $(G_4C_2)_2$/EGFP- and EGFP-expressing control neurons (Figure 3E and 3F and Table S1). Consistently, $(G_4C_2)_{66}$/EGFP neurons fired markedly fewer AP spikes compared to control neurons in response to suprathreshold depolarizing current injections (Figure 3G and 3H and Table S1). Furthermore, mutant neurons exhibited significantly smaller membrane input resistance, suggesting that their capability to support repetitive AP firing was severely compromised (Figure 3I–3K and Table S1). Except for a slower AP decay in mutant Cg1 neurons and an increased fast after-hyperpolarization (fAHP) in mutant PL neurons, the overall AP waveform, resting potential, and membrane capacitance in both Cg1 and PL neurons were similar across groups (Table S1). Together, these results demonstrate a profound hypoexcitability in dmPFC LV pyramidal neurons in aged mutant mice.

In vivo dmPFC photoinhibition attenuates empathic function

To examine whether dmPFC hypoexcitability is responsible for the lost empathy in mutant mice, we inhibited dmPFC pyramidal neurons in wildtype mice and tested the effects on observational fear and other-directed comforting behaviors using *in vivo*

optogenetics[37]. AAVs encoding the inhibitory halorhodopsin eNpHR3.0 or mCherry were bilaterally injected into the dmPFC and chronic optic fibers were implanted above the target sites (Figure 4A and Figure S3A). *Ex vivo* electrophysiology confirmed markedly reduced AP firing (Figure S3B–S3D) and excitability (Figure S3E) in dmPFC pyramidal neurons expressing eNpHR3.0 in response to 593 nm LED illumination. A continuous laser stimulation (561 nm) was used to inhibit pyramidal neurons *in vivo* during HC2 (counterbalanced laser-ON-OFF or laser-OFF-ON schedules; Figure 4A). dmPFC photoinhibition potently attenuated other-directed affiliative behaviors in eNpHR3.0- but not mCherry-injected observers, with significantly shorter allogrooming and body contact duration, smaller bout numbers and longer latency during laser-ON compared to laser-OFF phases (Figure 4B–4I, Figure S3F–S3I and Video S2), regardless of ON-OFF or OFF-ON sequences (Figure S3J and S3K). dmPFC photoinhibition also significantly decreased observational fear in eNpHR3.0-injected mice compared to mCherry-injected mice (Figure 4J). Furthermore, dmPFC photoinhibition markedly attenuated other-directed affiliation in the non-observational DIA paradigm (Figure S3L–S3Q). In contrast, dmPFC inhibition did not affect locomotor activity or anxiety behavior in an open field (Figure S3R and S3S). Together, these experiments demonstrate that pyramidal neuron activity in the dmPFC is required for both vicarious fear and prosocial consolation in mice.

Rescue of empathic deficits in aged $(G_4C_2)_{66}$/EGFP mice

Finally, we examined whether increasing dmPFC excitability could rescue the lost empathy in aged $(G_4C_2)_{66}$/EGFP mice. We employed a chemogenetic approach[38] by delivering AAVs expressing the Gq-coupled stimulatory DREADD (designer receptor exclusively activated by designer drug) hM3Dq bilaterally into the dmPFC of aged $(G_4C_2)_{66}$/EGFP mice ($(G_4C_2)_{66}$/hM3Dq; Figure 4K) and activating infected neurons by the synthetic ligand clozapine-N-oxide (CNO). Slice electrophysiology confirmed that bath-application of CNO enhanced the excitability of hM3Dq-expressing dmPFC LV neurons by increasing spike numbers in response to current injections, depolarizing the resting potential and decreasing the minimal injected current needed to induce APs (Figure S4A–S4D). Using a within-subject, counterbalanced drug-administration design in the observational DIA paradigm (Figure S4E), we found that CNO, but not saline, treatments rescued both observational fear and other-directed affiliation in aged $(G_4C_2)_{66}$/hM3Dq observers, indicated by significantly increased affiliative duration and number of bouts and reduced latency in CNO-relative to saline-treated mice (Figure 4L–4N, Figure S4F, Video S2). Aged EGFP or $(G_4C_2)_{66}$/EGFP mice transduced with control AAVs showed similar empathic responses after saline or CNO treatments (Figure 4L-4N, Figure S4F–S4J). Activating dmPFC more selectively during HC2 by timed CNO administration in a modified DIA assay showed a similar rescue of affiliative behavior in $(G_4C_2)_{66}$/hM3Dq mice, suggesting that this rescue was not due to potential observation and fear acquisition enhancement (Figure S4K–S4N). Furthermore, chemogenetic dmPFC activation rescued other-directed affiliative behavior in the non-observational DIA paradigm (Figure S4O–S4Q). Finally, dmPFC activation did not affect general locomotor activity in $(G_4C_2)_{66}$/hM3Dq mice in the open field (Figure S4R), suggesting that the hyperlocomotion was not caused by dmPFC hypoactivity and was unlikely to contribute to empathy deficits in mutant mice. Together, we conclude that dmPFC hypoactivity underlies the empathic deficits in aged $(G_4C_2)_{66}$/EGFP mice.

DISCUSSION

It is now appreciated that evolutionarily conserved forms of human empathy are expressed by rodents[2,3]. Here we have developed a mouse empathy paradigm that captures both emotional contagion and ensuing prosocial consolation, two foundational empathic processes in the multilayered Russian-doll model of empathy[1]. Whereas observational fear has been extensively studied as a model of emotional contagion in mice[3], consolation-related allogrooming, initially documented in the highly social and monogamous prairie vole[7], was reported in mice only recently[9]. Other-oriented body contact (aka physical proximity) is an affiliative behavior thought to afford comforting and strengthen social bonding in group-housed rodents[39] but has not been shown in a prosocial consolation context. Our results thus uncover a previously undocumented empathy-driven caring behavior in rodents. Somewhat counterintuitive but not surprisingly, other-directed consolation does not solely depend on prior vicarious fear in our observational DIA paradigm, consistent with studies that other sensory modalities, e.g. olfactory cues from distressed conspecifics, may elicit affiliative behaviors[9,40]. The extent and mechanisms of how various sensory inputs may impact resulting affiliative responses warrant future investigations.

Our findings that dmPFC regulates both observational fear and prosocial consolation expand the rodent empathy circuits along the anterior-posterior axis of the ACC as dmPFC, equivalent of the rostral portion of ACC in the ACC/MCC nomenclature[41], resides more anterior to the classical ACC involved in rodent empathy[42,43]. The dmPFC plays intricate roles in social cognition[44,45] and its anatomical homologue constitutes a node of cognitive empathy in humans[13,14,46]. Importantly, the dmPFC regulates both observational and non-observational aspects of empathy, consistent with its position as a central hub that evaluates and integrates information arrived from diverse sensory routes to direct behaviors[47]. Interestingly, a medial amygdala (MeA)-hypothalamus circuit deep in the social behavioral network encodes and drives prosocial allogrooming in an acute, time-locked manner[9], whereas the dmPFC likely regulates affiliative behaviors via top-down-related mechanisms. These works provide a foundation to further delineate cellular and circuit mechanisms of various faces of empathy and empathy-driven behaviors.

Loss of empathy is a cardinal symptom of bvFTD[20–22] and is seen in other psychiatric and neurological diseases[18,19], but neither an animal model nor an underlying neural mechanism has been described for any disease so far. Here, we develop a mouse model of bvFTD that exhibits striking impairments of two basic forms of empathy, affect-sharing and prosocial comforting, and displays profound dmPFC hypoexcitability. Importantly, this dmPFC hypoactivity is both necessary and sufficient for empathy loss in mutant animals. We propose that functional hypoactivity, independent of a structural atrophy, can serve as a pathophysiological mechanism for impaired empathy in bvFTD. We speculate that reduced spiking of empathy/affect-encoding dmPFC cells compromise their capacity to detect, integrate and process inputs that carry sensory, social, and emotional information and/or to output/transfer this information to downstream targets during empathic behaviors.

Altered neuronal excitability, particularly hyperexcitability, is frequently associated with neurodegenerative diseases and often serves as a diagnostic feature and/or pathological

driver[48–50]. For instance, motor cortex hyperexcitability at pre-symptomatic stages of ALS has been hypothesized to drive motor neuron death via dying-forward trans-synaptic excitotoxicity[48]. Consistently, motoneurons derived from C9ALS patient induced pluripotent stem cells display an early hyperexcitability[51–53] followed by a late-stage hypoexcitability[52]. The excitability states of PFC neurons in FTD are unknown. Our study provides *in vivo* evidence that prefrontal neurons are profoundly hypoactive at a symptomatic stage of FTD. This hypoexcitability manifests primarily as reduced firing capacity associated with reduced input resistance, suggesting potential alterations of subthreshold-operating ion channels. Although the pathologic trajectory leading to the hypoexcitable state and the underlying ionic basis and regional specificity remain unknown, this hypoexcitability likely represents a late-stage functional inactivation. Remarkably, mitigating this hypoexcitability is effective to restore empathy even at an advanced disease stage with substantial neurodegeneration. Thus, enhancing the activity of the frontotemporal cortex may serve as a viable therapeutical strategy for bvFTD, for which there are currently no approved, and few effective, treatments[54]. Finally, our study has implications in understanding and ameliorating the deterioration of empathy that manifests in other brain diseases and that of which appears to permeate our world today.

STAR METHODS

RESOURCE AVAILABILITY

Lead Contact—Further information and requests for resources and reagents should be directed to and will be fulfilled by the lead contact, Wei-Dong Yao (yaow@upstate.edu).

Materials Availability—All data are available in the main text or supplementary materials. Requests for resources and additional information should be directed to and will be fulfilled by the lead contact. This study did not generate unique reagents.

Data and Code Availability

- All data are available in the main text or supplementary materials and will be shared by the lead contact upon request.
- This paper does not report original code.
- Any additional information required to reanalyze the data reported in this paper is available from the lead contact upon request.

EXPERIMENTAL MODEL AND SUBJECT DETAILS

Age-matched (6–8 months or 12–14 months) male and female C57BL/6J mice (Jackson Laboratory) were used for all experiments. Both male and female mice were used, because no sex dependent differences were detected throughout these studies. Mice were group-housed 2–4 mice per cage under a 12 h light/dark cycle (8:00–20:00 light) with access to standard chow food and water *ad libitum*. The animal housing facility maintains a temperature of 21–23 °C and a humidity of 30–70%. All animal studies and experimental procedures were approved by the Institutional Animal Care and Use Committee of SUNY

Upstate Medical University and conducted in accordance with the National Institutes of Health “Guidelines for the Care and Use of Laboratory Animals.”

METHOD DETAILS

Surgeries

Neonatal Intracerebroventricular (ICV) Viral Injections: Postnatal day 0 (p0) mice were cryoanesthetized on ice for approximately 3 minutes or until there was no movement. A 32-gauge needle was attached to a 10 μL syringe (Hamilton Company) to manually deliver 2 μL of AAV9-$(G_4C_2)_2$ or AAV9-$(G_4C_2)_{66}$ mixed with 2 μL of AAV9-EGFP or 2 μL of AAV9-EGFP alone. The syringe was inserted at a 30° angle approximately two-fifths the distance between the lambda suture and each eye and held at a depth of approximately 2 mm[29]. Immediately following injections, the pups were placed on a heating pad to recover before being placed back into their home cages. For all injections, mice were randomly assigned.

Stereotactic Surgeries: Surgical procedures were conducted with a small animal stereotaxic apparatus (Kopf Instruments) under aseptic conditions. Mice were anesthetized with isoflurane (5% for induction, 1.5%−2% for maintenance) and placed in the stereotaxic apparatus. Two small bilateral burr holes were made directly above the injection sites using a dental drill. Bilateral viral injections (0.4 μL) were made with a 32 gauge 1.0 μL Neuros syringe (Hamilton Company) at a rate of 0.05 μL min^{-1} using an ultraprecise micromanipulator (Stoelting Company) into the dmPFC (anterior/posterior (AP), +1.94 mm; medial/lateral (ML), +/−.375 mm; dorsal/ventral (DV), −1.70 mm from Bregma). Following injections, needles were left in place for 10 minutes to assure complete delivery of the virus.

For optogenetic experiments performed with *in vivo* photostimulation, bilateral viral injections (0.25–0.4 μL) were made with a 32 gauge 1.0 μL Neuros syringe at a rate of 0.05 μL min^{-1} into two different dmPFC subregions, Cg1 (AP, +2.04 mm to +1.94 mm; ML, +/−.750 mm; DV, −1.45 mm to −1.65 mm from Bregma; 10° angle) or PL (AP, +2.04 mm to +1.94 mm; ML, +/−.750 mm; DV, −1.75 mm from Bregma; 10° angle). Using a stereotaxic cannula holder (Thorlabs), mono fiber optic cannulas (200 μm, 0.37 NA, Doric Lenses) were then bilaterally implanted 0.25–0.45 mm above virus injection (photostimulation) sites in Cg1 (AP, +2.04 mm to +1.94 mm; ML, +/−.750 mm; DV, −1.2 mm from Bregma; 10° angle) or PL (AP, +2.04 mm to +1.94 mm; ML, +/−.750 mm; DV, −1.45 mm from Bregma; 10° angle). We separately targeted the two subregions to ensure that the dmPFC was adequately covered and effectively photostimulated with localized optic fibers, and to reveal potential subregion-dependent differences in behaviors. Identical coordinates and viral volumes were used in all mice within the same experimental cohorts. No differences in behaviors were found thus data from Cg1 and PL were combined. To anchor the implants to the skull several layers of industrial strength dental grip cement (Dental Supply) were placed between the implants and dried skull creating a cement cap. After surgery, Neosporin was applied liberally around the cement cap.

Open incisions were closed securely using Vetbond Tissue Adhesive (3M) and each mouse received a subcutaneous injection of Buprenorphine (0.1 mg kg^{-1}) as a post-operative

analgesic. Locations of virus injections and fiber implants were verified postmortem by histology.

Behavioral Assays—All behavioral assays were performed on age-matched 6–8-month-old (Figure 1, Figure 3A–3C, Figure 4A–4J, Figure S1, Figure S3 and Videos S1 and S2) or 12–14-month-old (Figure 2, Figure 3D–3K, Figure 4K–4N, Figure S2, Figure S4, Table S1 and Videos S1 and S2) male and female mice during the animals' light cycle. Behavioral equipment was illuminated with an overhead light (440 lux) and cleaned with Rescue disinfectant prior to use with each animal. Mice were habituated to the testing room 1–2 days prior to the start of testing and 1 hour before each test and returned to their home cages at the conclusion of each test. Animals were allowed 1–2 days of rest between different behavioral assays. All tests were recorded with a Noldus EthoVision XT video-tracking system and analyzed offline. Mice were randomly assigned to individual experimental groups.

Distress-induced Affiliation (DIA) Test: Before testing, all cage mates were temporarily moved to a holding cage and each test mouse (observer) was allowed 1 minute to explore its homecage under overhead lighting (440 lux). Behavioral testing was performed in the observers' homecage (covered with a cage lid unless otherwise noted) to minimize novelty- or stress-induced behaviors. An unfamiliar 6–12-month-old same-sex wild-type C57BL/6J mouse (demonstrator) was then introduced into the cage and allowed to freely interact with the observer for 10 minutes (homecage 1, HC1 test). Immediately following the HC1 interaction test, the demonstrator mouse was placed into a transparent, single-chamber fear-conditioning apparatus with a stainless-steel rod shock floor (Med Associates) and the observer mouse was placed into an adjacent identical transparent apparatus. As such, the observing mouse could sense visual, auditory and olfactory cues from the demonstrator as it was subjected to repetitive foot shocks. The observation fear conditioning (OFC) phase began with 5 minutes of habituation (no foot shocks) followed by 4 minutes of repetitive foot shocks (2 ms each, 1.0 mA, 10 s intervals, 20 total) to the demonstrator delivered manually by a shocker/scrambler module (Med Associates), a protocol previously shown to elicit homogenous behavioral responses (running, vocalizing and jumping)[5]. Immediately following OFC, the mice were placed back into the observer's homecage and post-shock behavior was recorded for 10 minutes (homecage 2, HC2 test). To assess contextual fear retrieval, observer mice were placed back into the fear-conditioning chamber 24-hours post-conditioning (without demonstrators) for 4 minutes and freezing responses were measured.

For the DIA assay without OFC (non-observational DIA), observer mice were moved to an isolated holding area after HC1 while demonstrators were subjected to 4 minutes of repetitive foot shocks (2 ms, 1.0 mA, 10 s intervals, 20 total). Immediately following foot shocks, demonstrators were reunited with observer mice and post-shock behavior was recorded for 10 minutes (HC2 test).

Videos recorded from DIA experiments were manually scored (unless otherwise noted) for an array of behaviors using ANY-Maze software. The following behavioral parameters were measured: (i) Time freezing by observer mice during OFC. Freezing behavior was quantified automatically by ANY-Maze tracking software, unless otherwise noted.

Motionless bouts with a minimum duration of 1 s were considered a freeze. (ii) Affiliative behaviors (allogrooming and body contact) by observer mice during HC1 and HC2 tests. Allogrooming was defined as visible licking and/or mouth contact on the body trunk, shoulder region and/or head of the demonstrator mouse by the observer mouse that was accompanied by head bobbing indicative of licking motions (Video S1). Body contact was measured as whole or partial body contact, initiated by the observer mouse, with a minimum onset duration of 1 s (Video S1). For quantification of allogrooming or body contact number of bouts, consecutive bouts with < 1 s interval between them were considered to be one continuous bout. (iii) Social investigation behaviors of observer mice during HC1 and HC2 tests, including head, body, and anogenital sniffing. Sniffing was defined as nose contact with the demonstrator, without body contact. (iv) Non-social behaviors of observer mice during HC1 and HC2 tests, including rearing, self-grooming, inactive and locomotion. Inactive behaviors were defined as cessation of all movements and included sleeping and still and alert behaviors as advocated at https://conductscience.com/maze/resources/mouse-ethogram/inactive-behaviors-overview/. (v) Allogrooming, social approach, and immobility behaviors of demonstrator mice during HC1 and HC2 tests. Social approach was defined as a sequence of behaviors initiated by the demonstrator that began with locomotor or non-social behavior followed by an approach toward the observer that ultimately led to social investigation or allogrooming. Motionless bouts lasting longer than 1 s were scored as time immobile.

Open Field: Mice were placed in the center of a square arena (40 cm x 40 cm x 30 cm, Med Associates) illuminated by an overhead light (440 lux) and allowed to freely explore for 60 min. A video camera was placed directly above the apparatus to track the movement of each animal (ANY-Maze, Stoelting). Parameters measured included total distance travelled and time spent in the center zone (20 × 20 cm) of the apparatus. Heat maps were constructed as the cumulative time spent within a unit area defined in ANY-Maze software. A ratio of total distance travelled in the center zone to total distance travelled over the entire apparatus (center-to-total distance ratio) was calculated as an indication of anxiety. In experiments assaying the stress-reducing effects on demonstrator mice following the DIA test, demonstrators were subjected to one 30-minute open field test 24 hours prior to the DIA test (baseline) and immediately after (within 1 minute) HC2 test in which they were either alone or reunited with an observer. Center-to-total distance ratio was measured as described above at baseline and post-shock to assess changes in anxiety levels.

Olfactory Function: Following a 5-minute habituation to empty cages with no bedding, mice were tested for both odor discrimination and sensitivity. In the discrimination task, mice were challenged with two filter papers (2 × 2 in) placed in opposite ends of the cage. One was embedded with either an attractive scent (vanilla or cinnamon) or an aversive scent (2-methyl-butyrate) and the other with a neutral scent (water). The mice were tested in three consecutive 3-minute trials where they explored the three scent pairs (vanilla-water, cinnamon-water, 2-methyl-butyrate-water). The amount of time spent sniffing the neutral scent was subtracted from the amount of time spent sniffing the aversive or attractive scents as an indicator of scent discrimination. For the sensitivity assay, we compiled the amount of time spent sniffing one piece of filter paper embedded with a neutral scent (water) vs. one

piece of filter paper embedded with vanilla scent at three different dilutions (10^1, 10^2 and 10^3) in three consecutive 3-minute trials.

Water Spray: Before testing, all cagemates were temporarily moved to a holding cage and each test mouse was allowed 1 minute to explore its homecage under overhead lighting (440 lux). The mouse was then removed from their homecage, sprayed with a single mist of double-distilled water and placed back into its homecage. Self-grooming behaviors included manual grooming, oral grooming and/or scratching were measured for 15 minutes.

***In vivo* Chemogenetics:** *In vivo* chemogenetic behavioral experiments were performed 2–4 weeks post-surgery, allowing for adequate expression of viral proteins and full recovery from surgery. Mice were handled and acclimated to intraperitoneal (i.p.) injections of saline (as vehicle control) 3–5 days prior to behavioral testing. Each mouse received two trials of behavioral tests counterbalanced with either CNO (1 mg kg^{-1}) or saline. Specifically, mice were selected randomly to receive i.p. injections of CNO or saline for the first trial of behavior experiments followed by the reverse order (saline or CNO) for the second trial of behavioral tests two weeks later. CNO or saline injections were administered 20 minutes prior to the start of each behavioral test.

To specifically activate dmPFC during HC2 without potential compounding effects of OFC, we used a modified observational DIA paradigm (Figure S4K). Specifically, observer mice were administered CNO immediately after OFC and placed alone in their homecages for 20 minutes prior to HC2 test. Demonstrators were re-shocked (without observer witnessing) for 2 minutes (2 ms each, 1.0 mA, 10 s intervals, 10 total) to ensure their states of distress immediately before they were reunited with CNO-injected observers in HC2.

***In vivo* Optogenetics:** *In vivo* optogenetic behavioral experiments were performed 2–4 weeks post-surgery, allowing for adequate expression of viral proteins and full recovery from surgery. Mice were handled and acclimated to attached 1-m fiber patch cables (200 μm, 0.39 NA, Thorlabs) 3–5 days prior to behavioral testing. Using a 561 nm DPSS laser (Opto Engine LLC), each mouse received two trials of observational or non-observational DIA behavioral tests counterbalanced with either laser ON for 4 minutes (10–15 mW output) then OFF for 4 minutes or laser OFF then ON in HC2. Specifically, mice were selected randomly to receive light ON for the first half of HC2 in DIA followed by light OFF for the second half of the test. Two weeks later, during the second trial of behavioral tests, the sequence of light stimulation was reversed. To analyze DIA behaviors (Figure 4B–4I), HC2 light OFF phase (minutes 1–4 or minutes 4–8) was compared to corresponding HC1 light OFF phase (minutes 1–4 or minutes 4–8). Similarly, HC2 light ON phase (minutes 1–4 or minutes 4–8) was compared to HC1 light OFF phase (minutes 1–4 or minutes 4–8). DIA behaviors were then averaged between the two counterbalanced trials. In OFC optogenetics experiments (Figure 4J), eNPHR3.0- and mCherry-transduced observers were subjected to a 5-minute baseline (light OFF) followed by a 4 minute photoinhibition (light ON). Freezing responses were manually scored and analyzed. In open field tests, mice were subjected to a 15-minute test with a light OFF (5 minutes) -ON (5 minutes) -OFF (5 minutes) schedule. For analysis, data recorded during the two light OFF phases were averaged and compared to light ON phase.

Brain Slice Electrophysiology

Brain Slice Preparation: 12- to 14-month-old $(G_4C_2)_{66}$/EGFP mice, $(G_4C_2)_2$/EGFP and EGFP control littermates were sacrificed and their brains rapidly removed and placed into ice-cold artificial cerebrospinal fluid (ACSF) that contained the following (in mM): 126 NaCl, 2.5 KCl, 2.5 $CaCl_2$, 1.2 $MgCl_2$, 25 $NaHCO_3$, 1.2 NaH_2PO_4 and 11 D-glucose. Coronal cortical slices (300 um) containing the dmPFC (including PL and Cg1) were cut using a vibratome (Leica) and superfused with ice-cold ACSF that was saturated with 95% O2 and 5% CO2. Brain slices were incubated at room temperature (21–23 °C) for at least 1 hour prior to being transferred to a recording chamber continuously perfused with oxygenated ACSF and maintained at 32 °C with a temperature controller (Warner Instruments). All drugs used in this study were delivered to the bath by a gravity-driven perfusion system (Harvard Apparatus).

Electrophysiology: Whole-cell patch-clamp electrophysiology was performed as previously described[55–57]. Current-clamp recordings were performed on EGFP- or mCherry-positive dmPFC LV pyramidal neurons that were identified by their characteristic morphology and adaptive firing patterns in response to suprathreshold depolarizing current injections. Recording pipettes (3.5–4.5 MΩ) were filled with the following (in mM): 130 K-gluconate, 8 NaCl, 10 HEPES, 0.4 EGTA, 2 Mg-ATP, and 0.25 GTP-Tris, pH 7.25. Picrotoxin (50 μM) was included in the superfusion medium to block GABAA receptor-mediated inhibitory responses. All recordings were made at resting membrane potential using a Multiclamp 700B amplifier (Molecular Devices). Cells with a resting membrane potential > −55 mV or that became depolarized > −55 mV during recordings were excluded from analysis. To assess intrinsic excitability and AP waveform properties, we used a depolarizing step-current injection protocol that delivered a series of 500 ms, +25 pA current steps from −35 pA to 440 pA (20 steps) at 10 s inter-sweep intervals. To characterize input resistance, we injected a series of hyperpolarizing currents of 500 ms, −25 pA current steps at 10 s inter-sweep intervals from 0 pA to −200 pA (9 steps).

Resting membrane potential (RMP) was measured with no current injected under current clamp. The first AP elicited by minimal injected currents was used to measure active membrane properties. AP threshold was measured at the inflexion point during take-off. AP amplitude was measured as the membrane potential difference between the point of AP take-off and the peak. Rise and decay slope were calculated by measuring the slope of the AP upstroke (rise) and downstroke (decay). AP half-width was measured at half AP amplitude. Fast afterhyperpolarization (fAHP) was measured as the membrane potential difference between AP threshold and peak hyperpolarization. Medium AHP (mAHP) was measured as the membrane potential difference between AP threshold and the second peak hyperpolarization (where possible). Slow AHP (sAHP) was measured as the peak hyperpolarization (relative to resting membrane potential) at the conclusion of a train of APs induced by current injection.

To confirm chemogenetic manipulation of neuronal activity in the dmPFC using slice electrophysiology, 2–4-month-old C57BL/6J wildtype mice were sacrificed 2–4 weeks after AAV2-hM3D(Gq)-mCherry injection. Whole-cell current-clamp recordings were performed

on visually identified neurons expressing hM3Dq-mCherry. Baseline resting membrane potential, spontaneous activity at resting, and AP firing evoked by depolarizing step current injections were measured as described above. CNO (5 μM) was then applied to the bath and recordings of both resting and evoked activities were repeated.

To confirm optogenetic manipulation of neuronal activity in the dmPFC using slice electrophysiology, 2–4-month-old C57BL/6J wildtype mice were sacrificed 2–4 weeks after AAV5-eNpHR3.0-mCherry injection. Whole-cell current-clamp recordings were performed on visually identified neurons expressing eNpHR3.0-mCherry. Baseline AP firing was recorded by delivering a series of 500 ms-depolarizing currents with a +25 pA increments (−35 pA to 440 pA, 20 steps) at 10 s intervals. After the baseline was established, a second step-current injection test was recorded (−35 pA to 440 pA, 20 steps, 500 ms) in the absence (250 ms) followed by the presence (250 ms) of 593 nm LED light stimulations as generated from a CoolLED pE-300ultra fluorescence microscopy illumination system controlled by TTL input and delivered through a 40 X objective.

Data acquisition and analysis were carried out using Digidata 1322A and pClamp software (version 9.2; Molecular Devices). All signals were digitized at 20 kHz and filtered off-line at 2 kHz. Series resistance was monitored throughout the whole-cell recordings and data were discarded if the resistance changed by >15%.

Immunohistochemistry, Histology and Imaging Analysis—Animals were either perfused or drop fixed with 4% paraformaldehyde (PFA) in PBS. To quantify immediate early gene (IEG) c-Fos expression activated during behavior, mice were sacrificed 60–90 minutes after conclusion of behavior tests. Coronal (for c-Fos experiments) or mid-sagittal (for NeuN experiments) brain slices were cut at 40–50 μm with a vibratome (Leica 1000 Plus Sectioning System), washed in PBS for 10 minutes (3 times) and permeabilized and blocked for 2 hours at room temperature with blocking solution: 1% Triton X-100 (Sigma) and 10% goat serum (Invitrogen) in PBS. Sections were then washed in PBS and incubated with primary antibody for 20 minutes at room temperature, then at 4 °C overnight in antibody solution: 0.1% Triton X-100 (Sigma) and 5% goat serum (Invitrogen) in PBS. Next day sections were washed in PBS and incubated with secondary antibody for 2 hours at room temperature in antibody solution. Finally, sections were washed in PBS, mounted on Superfrost Plus slides (Fisher Scientific), air dried and coverslipped. For c-Fos immunostaining, sections were mounted with Prolong Gold Antifade with DAPI (Invitrogen). For NeuN immunostaining, sections were mounted with CC/Mount tissue mounting medium (Sigma). For poly(GR) and poly(GA) immunostaining, slices were stained with Hoechst (Invitrogen) and mounted with CC/Mount tissue mounting medium (Sigma).

Antibodies used and dilutions are as follows: rabbit anti-c-Fos (1:1000, Synaptic Systems), rabbit anti-NeuN (1:1000, Millipore), rabbit anti-C9ORF72/C9RANT (poly-GR) (1:2,000, Millipore), rabbit anti-$(GA)_8$ (1:2,000, Covance), mouse anti-GFP (1:1,000, Novus) and Alexa Fluor 488, 555 and 568 secondary antibodies (1:500, Invitrogen).

Confocal images of NeuN- and DPR-stained sections were acquired with a Zeiss LSM 800 confocal microscope and processed with Zeiss Zen software. Confocal images of c-Fos-stained tissues were acquired using an Olympus Fluoview FV1000 confocal microscope and processed using automated mosaic stitch image acquisition (Olympus FV1000 software). For cell counting, high-resolution images of the dmPFC were acquired using a 20 X oil-immersion objective. Brain regions were then defined by overlaying confocal images with corresponding brain section images from the Mouse Brain Atlas [58]. NeuN- and c-Fos-positive cells were counted manually (ImageJ software) from 3–4 slices per mouse (3–4 animals per condition) containing regions of interest. Analyses were performed by investigators who were not blind to experimental conditions.

To confirm localization of virus injections and optic fiber implants, brains were processed, cut (50 μm) and mounted (Prolong Gold Antifade without DAPI, Invitrogen) as described above. Fluorescent images were acquired with an Olympus CKX53 fluorescent microscope using a 4X objective and processed with ImageJ software. Injection locations were verified in the dmPFC (Cg1 or PL) by presence of EGFP or mCherry fluorescence. Optic fiber locations in the dmPFC were identified by fiber tracks.

QUANTIFICATION AND STATISTICAL ANALYSIS

Data are shown as mean ± s.e.m. Animals were excluded if they became sick or died before completion of behavioral or *in vivo* chemogenetic or optogenetic tests, or if *post hoc* histological analysis showed inaccurate placement of virus injections or optic fiber implants. Two-sided paired Student's *t*-tests were used for within-group comparison of two treatments and two-sided unpaired Student's *t*-tests for comparison between two groups. One-way ANOVA with Bonferonni's multiple comparison post-hoc tests were performed to assess significance for multiple group comparisons and two-way ANOVA with Bonferonni's multiple comparison post-hoc tests for multiple group comparisons across multiple time points. NS, not significant. $^{*}P < 0.05$, $^{**}P < 0.01$, $^{***}P < 0.001$ vs. EGFP and $(G_4C_2)_2$/EGFP, where notation indicates the least significant *P* value of both comparisons. $^{\#}P < .05$, $^{\#\#}P < .01$, $^{\#\#\#}P < .001$ vs. $(G_4C_2)_2$/EGFP. Detailed information regarding sample sizes, statistical test types, *P* values and test statistics are summarized in Table S2. All statistical analyses were performed using Prism 6.0 (GraphPad Software). Sample sizes were not predetermined using statistical methods. Experiments were randomized where possible. Experimenters were not blind to group allocation.

Supplementary Material

Refer to Web version on PubMed Central for supplementary material.

Acknowledgments:

We thank C. Morel and X. Sun for assistance with in vivo optogenetics, Y. Lin for comments, and members of the Yao laboratory for valuable discussions. This work was supported by NIH grants R01MH106489, R56NS122351, and R21NS125845 (to W.-D.Y.), R01NS093097 (to W.-D.Y. and F.-B.G.), R37NS057553 and R01NS101986 (to F.-B.G.), R35NS097273, U54NS123743, and P01NS084974 (to L.P.), and NIH fellowship F31NS108579 (to H.L.P.).

REFERENCES

1. Waal F.B.M. de (2008). Putting the Altruism Back into Altruism: The Evolution of Empathy. Annu Rev Psychol 59, 279–300. 10.1146/annurev.psych.59.103006.093625. [PubMed: 17550343]
2. Panksepp JB, and Lahvis GP (2011). Rodent empathy and affective neuroscience. Neurosci Biobehav Rev 35, 1864–1875. 10.1016/j.neubiorev.2011.05.013. [PubMed: 21672550]
3. Kim S-W, Kim M, and Shin H-S (2021). Affective empathy and prosocial behavior in rodents. Curr Opin Neurobiol 68, 181–189. 10.1016/j.conb.2021.05.002. [PubMed: 34091136]
4. Langford DJ, Crager SE, Shehzad Z, Smith SB, Sotocinal SG, Levenstadt JS, Chanda ML, Levitin DJ, and Mogil JS (2006). Social Modulation of Pain as Evidence for Empathy in Mice. Science 312, 1967–1970. 10.1126/science.1128322. [PubMed: 16809545]
5. Jeon D, Kim S, Chetana M, Jo D, Ruley HE, Lin S-Y, Rabah D, Kinet J-P, and Shin H-S (2010). Observational fear learning involves affective pain system and Cav1.2 Ca2+ channels in ACC. Nat Neurosci 13, 482–488. 10.1038/nn.2504. [PubMed: 20190743]
6. Li Z, Lu Y-F, Li C-L, Wang Y, Sun W, He T, Chen X-F, Wang X-L, and Chen J. (2014). Social interaction with a cagemate in pain facilitates subsequent spinal nociception via activation of the medial prefrontal cortex in rats. Pain 155, 1253–1261. 10.1016/j.pain.2014.03.019. [PubMed: 24699208]
7. Burkett JP, Andari E, Johnson ZV, Curry DC, Waal F.B.M. de, and Young LJ (2016). Oxytocin-dependent consolation behavior in rodents. Science 351, 375–378. 10.1126/science.aac4785. [PubMed: 26798013]
8. Smith ML, Asada N, and Malenka RC (2021). Anterior cingulate inputs to nucleus accumbens control the social transfer of pain and analgesia. Science 371, 153–159. 10.1126/science.abe3040. [PubMed: 33414216]
9. Wu YE, Dang J, Kingsbury L, Zhang M, Sun F, Hu RK, and Hong W. (2021). Neural control of affiliative touch in prosocial interaction. Nature 599, 262–267. 10.1038/s41586-021-03962-w. [PubMed: 34646019]
10. Bartal IB-A, Decety J, and Mason P. (2011). Empathy and Pro-Social Behavior in Rats. Science 334, 1427–1430. 10.1126/science.1210789. [PubMed: 22158823]
11. Apps MAJ, Rushworth MFS, and Chang SWC (2016). The Anterior Cingulate Gyrus and Social Cognition: Tracking the Motivation of Others. Neuron 90, 692–707. 10.1016/j.neuron.2016.04.018. [PubMed: 27196973]
12. Carrillo M, Han Y, Migliorati F, Liu M, Gazzola V, and Keysers C. (2019). Emotional Mirror Neurons in the Rat's Anterior Cingulate Cortex. Curr Biol 29, 1301–1312.e6. 10.1016/j.cub.2019.03.024. [PubMed: 30982647]
13. Engen HG, and Singer T. (2013). Empathy circuits. Curr Opin Neurobiol 23, 275–282. 10.1016/j.conb.2012.11.003. [PubMed: 23219409]
14. Waal F.B.M. de, and Preston SD (2017). Mammalian empathy: behavioural manifestations and neural basis. Nat Rev Neurosci 18, 498–509. 10.1038/nrn.2017.72. [PubMed: 28655877]
15. Allsop SA, Wichmann R, Mills F, Burgos-Robles A, Chang C-J, Felix-Ortiz AC, Vienne A, Beyeler A, Izadmehr EM, Glober G, et al. (2018). Corticoamygdala Transfer of Socially Derived Information Gates Observational Learning. Cell 173, 1329–1342.e18. 10.1016/j.cell.2018.04.004. [PubMed: 29731170]
16. Terranova JI, Yokose J, Osanai H, Marks WD, Yamamoto J, Ogawa SK, and Kitamura T. (2022). Hippocampal-amygdala memory circuits govern experience-dependent observational fear. Neuron 110, 1416–1431.e13. 10.1016/j.neuron.2022.01.019. [PubMed: 35139362]
17. Zhang M-M, Geng A-Q, Chen K, Wang J, Wang P, Qiu X-T, Gu J-X, Fan H-W, Zhu D-Y, Yang S-M, et al. (2022). Glutamatergic synapses from the insular cortex to the basolateral amygdala encode observational pain. Neuron 110, 1993–2008.e6. 10.1016/j.neuron.2022.03.030. [PubMed: 35443154]
18. Brambati SM, Myers D, Wilson A, Rankin KP, Allison SC, Rosen HJ, Miller BL, and Gorno-Tempini ML (2006). The Anatomy of Category-specific Object Naming in Neurodegenerative Diseases. J Cognitive Neurosci 18, 1644–1653. 10.1162/jocn.2006.18.10.1644.

19. Decety J, and Moriguchi Y. (2007). The empathic brain and its dysfunction in psychiatric populations: implications for intervention across different clinical conditions. Biopsychosoc Medicine 1, 22. 10.1186/1751-0759-1-22.
20. Neary D, Snowden J, and Mann D. (2005). Frontotemporal dementia. La Press Médicale 4, 771—780. 10.1016/j.lpm.2007.04.023.
21. Olney NT, Spina S, and Miller BL (2017). Frontotemporal Dementia. Neurol Clin 35, 339–374. 10.1016/j.ncl.2017.01.008. [PubMed: 28410663]
22. Snowden JS (2018). Empathy in Frontotemporal Dementia. Cogn Behav Neurol 31, 111. 10.1097/wnn.0000000000000156. [PubMed: 29927802]
23. Gao F, Almeida S, and Lopez-Gonzalez R. (2017). Dysregulated molecular pathways in amyotrophic lateral sclerosis–frontotemporal dementia spectrum disorder. Embo J 36, 2931–2950. 10.15252/embj.201797568. [PubMed: 28916614]
24. Renton AE, Majounie E, Waite A, Simón-Sánchez J, Rollinson S, Gibbs JR, Schymick JC, Laaksovirta H, Swieten JC van, Myllykangas, L., et al. (2011). A hexanucleotide repeat expansion in C9ORF72 is the cause of chromosome 9p21-linked ALS-FTD. Neuron 72, 257–268. 10.1016/j.neuron.2011.09.010. [PubMed: 21944779]
25. DeJesus-Hernandez M, Mackenzie IR, Boeve BF, Boxer AL, Baker M, Rutherford NJ, Nicholson AM, Finch NA, Flynn H, Adamson J, et al. (2011). Expanded GGGGCC Hexanucleotide Repeat in Noncoding Region of C9ORF72 Causes Chromosome 9p-Linked FTD and ALS. Neuron 72, 245–256. 10.1016/j.neuron.2011.09.011. [PubMed: 21944778]
26. Ling SC, Polymenidou M, and Cleveland DW (2013). Converging mechanisms in als and FTD: Disrupted RNA and protein homeostasis. Neuron 79, 416—438. 10.1016/j.neuron.2013.07.033. [PubMed: 23931993]
27. Dunfield KA (2014). A construct divided: prosocial behavior as helping, sharing, and comforting subtypes. Front Psychol 5, 958. 10.3389/fpsyg.2014.00958. [PubMed: 25228893]
28. Roberson ED (2012). Mouse models of frontotemporal dementia. Ann Neurol 72, 837–849. 10.1002/ana.23722. [PubMed: 23280835]
29. Chew J, Gendron TF, Prudencio M, Sasaguri H, Zhang Y-J, Castanedes-Casey M, Lee CW, Jansen-West K, Kurti A, Murray ME, et al. (2015). C9ORF72 repeat expansions in mice cause TDP-43 pathology, neuronal loss, and behavioral deficits. Science 348, 1151–1154. 10.1126/science.aaa9344. [PubMed: 25977373]
30. Zhu Q, Jiang J, Gendron TF, McAlonis-Downes M, Jiang L, Taylor A, Garcia SD, Dastidar SG, Rodriguez MJ, King P, et al. (2020). Reduced C9ORF72 function exacerbates gain of toxicity from ALS/FTD-causing repeat expansion in C9orf72. Nat Neurosci 23, 615–624. 10.1038/s41593-020-0619-5. [PubMed: 32284607]
31. Majounie E, Renton AE, Mok K, Dopper EGP, Waite A, Rollinson S, Chiò A, Restagno G, Nicolaou N, Simon-Sanchez J, et al. (2012). Frequency of the C9orf72 hexanucleotide repeat expansion in patients with amyotrophic lateral sclerosis and frontotemporal dementia: A cross-sectional study. Lancet Neurology 11, 323–330. 10.1016/s1474-4422(12)70043–1. [PubMed: 22406228]
32. Zhou T, Zhu H, Fan Z, Wang F, Chen Y, Liang H, Yang Z, Zhang L, Lin L, Zhan Y, et al. (2017). History of winning remodels thalamo-PFC circuit to reinforce social dominance. Science 357, 162–168. 10.1126/science.aak9726. [PubMed: 28706064]
33. Kingsbury L, Huang S, Wang J, Gu K, Golshani P, Wu YE, and Hong W. (2019). Correlated Neural Activity and Encoding of Behavior across Brains of Socially Interacting Animals. Cell 178, 429–446.e16. 10.1016/j.cell.2019.05.022. [PubMed: 31230711]
34. Liang B, Zhang L, Barbera G, Fang W, Zhang J, Chen X, Chen R, Li Y, and Lin D-T (2018). Distinct and Dynamic ON and OFF Neural Ensembles in the Prefrontal Cortex Code Social Exploration. Neuron 100, 700–714.e9. 10.1016/j.neuron.2018.08.043. [PubMed: 30269987]
35. Padilla-Coreano N, Batra K, Patarino M, Chen Z, Rock RR, Zhang R, Hausmann SB, Weddington JC, Patel R, Zhang YE, et al. (2022). Cortical ensembles orchestrate social competition through hypothalamic outputs. Nature 603, 667–671. 10.1038/s41586-022-04507-5. [PubMed: 35296862]
36. Sesack SR, Deutch AY, Roth RH, and Bunney BS (1989). Topographical organization of the efferent projections of the medial prefrontal cortex in the rat: An anterograde tract-tracing study

with Phaseolus vulgaris leucoagglutinin. J Comp Neurol 290, 213–242. 10.1002/cne.902900205. [PubMed: 2592611]

37. Zhang F, Wang L-P, Boyden ES, and Deisseroth K. (2006). Channelrhodopsin-2 and optical control of excitable cells. Nat Methods 3, 785–792. 10.1038/nmeth936. [PubMed: 16990810]
38. Roth BL (2016). DREADDs for Neuroscientists. Neuron 89, 683–694. 10.1016/j.neuron.2016.01.040. [PubMed: 26889809]
39. Rault J-L (2019). Be kind to others: Prosocial behaviours and their implications for animal welfare. Appl Anim Behav Sci 210, 113–123. 10.1016/j.applanim.2018.10.015.
40. Sterley T-L, and Bains JS (2021). Social communication of affective states. Curr Opin Neurobiol 68, 44–51. 10.1016/j.conb.2020.12.007. [PubMed: 33434768]
41. Heukelum S. van, Mars RB, Guthrie M, Buitelaar JK, Beckmann CF, Tiesinga PHE, Vogt BA, Glennon JC, and Havenith MN (2020). Where is Cingulate Cortex? A Cross-Species View. Trends Neurosci 43, 285–299. 10.1016/j.tins.2020.03.007. [PubMed: 32353333]
42. Paradiso E, Gazzola V, and Keysers C. (2021). Neural mechanisms necessary for empathy-related phenomena across species. Curr Opin Neurobiol 68, 107–115. 10.1016/j.conb.2021.02.005. [PubMed: 33756399]
43. Keum S, and Shin H-S (2019). Neural Basis of Observational Fear Learning: A Potential Model of Affective Empathy. Neuron 104, 78–86. 10.1016/j.neuron.2019.09.013. [PubMed: 31600517]
44. Grossmann T. (2013). The role of medial prefrontal cortex in early social cognition. Front Hum Neurosci 7, 340. 10.3389/fnhum.2013.00340. [PubMed: 23847509]
45. Bicks LK, Koike H, Akbarian S, and Morishita H. (2015). Prefrontal Cortex and Social Cognition in Mouse and Man. Front Psychol 6, 1805. 10.3389/fpsyg.2015.01805. [PubMed: 26635701]
46. Laubach M, Amarante LM, Swanson K, and White SR (2018). What, If Anything, Is Rodent Prefrontal Cortex? Eneuro 5, ENEURO.0315–18.2018. 10.1523/eneuro.0315-18.2018.
47. Euston DR, Gruber AJ, and McNaughton BL (2012). The Role of Medial Prefrontal Cortex in Memory and Decision Making. Neuron 76, 1057–1070. 10.1016/j.neuron.2012.12.002. [PubMed: 23259943]
48. Geevasinga N, Menon P, Özdinler PH, Kiernan MC, and Vucic S. (2016). Pathophysiological and diagnostic implications of cortical dysfunction in ALS. Nat Rev Neurol 12, 651–661. 10.1038/nrneurol.2016.140. [PubMed: 27658852]
49. Styr B, and Slutsky I. (2018). Imbalance between firing homeostasis and synaptic plasticity drives early-phase Alzheimer's disease. Nat Neurosci 21, 463–473. 10.1038/s41593-018-0080-x. [PubMed: 29403035]
50. Starr A, and Sattler R. (2018). Synaptic dysfunction and altered excitability in C9ORF72 ALS/FTD. Brain Res 1693, 98–108. 10.1016/j.brainres.2018.02.011. [PubMed: 29453960]
51. Sareen D, O'Rourke JG, Meera P, Muhammad AKMG, Grant S, Simpkinson M, Bell S, Carmona S, Ornelas L, Sahabian A, et al. (2013). Targeting RNA foci in iPSC-derived motor neurons from ALS patients with a C9ORF72 repeat expansion. Sci Transl Med 5, 208ra149–208ra149. 10.1126/scitranslmed.3007529.
52. Devlin A-C, Burr K, Borooah S, Foster JD, Cleary EM, Geti I, Vallier L, Shaw CE, Chandran S, and Miles GB (2015). Human iPSC-derived motoneurons harbouring TARDBP or C9ORF72 ALS mutations are dysfunctional despite maintaining viability. Nat Commun 6, 5999. 10.1038/ncomms6999. [PubMed: 25580746]
53. Wainger BJ, Kiskinis E, Mellin C, Wiskow O, Han SSW, Sandoe J, Perez NP, Williams LA, Lee S, Boulting G, et al. (2014). Intrinsic membrane hyperexcitability of amyotrophic lateral sclerosis patient-derived motor neurons. Cell Reports 7, 1–11. 10.1016/j.celrep.2014.03.019. [PubMed: 24703839]
54. Tsai RM, and Boxer AL (2016). Therapy and clinical trials in frontotemporal dementia: past, present, and future. J Neurochem 138, 211–221. 10.1111/jnc.13640. [PubMed: 27306957]
55. Choi SY, Lopez-Gonzalez R, Krishnan G, Phillips HL, Li AN, Seeley WW, Yao W-D, Almeida S, and Gao F-B (2019). C9ORF72-ALS/FTD-associated poly(GR) binds Atp5a1 and compromises mitochondrial function in vivo. Nat Neurosci 22, 851–862. 10.1038/s41593-019-0397-0. [PubMed: 31086314]

56. Xu T-X, Sotnikova TD, Liang C, Zhang J, Jung JU, Spealman RD, Gainetdinov RR, and Yao W-D (2009). Hyperdopaminergic Tone Erodes Prefrontal Long-Term Potential via a D2 Receptor-Operated Protein Phosphatase Gate. J Neurosci 29, 14086–14099. 10.1523/jneurosci.0974-09.2009. [PubMed: 19906957]

57. Ruan H, and Yao W-D (2017). Cocaine Promotes Coincidence Detection and Lowers Induction Threshold during Hebbian Associative Synaptic Potentiation in Prefrontal Cortex. J Neurosci 37, 986–997. 10.1523/jneurosci.2257-16.2016. [PubMed: 28123030]

58. Paxinos G, and Franklin KBJ (2001). The Mouse Brain in Stereotaxic Coordinates (Academic Press).

Highlights:

- Mice display dmPFC-dependent emotional contagion and other-directed consolation.
- Emotional contagion and other-directed consolation are blunted in aged c9FTD mice.
- Aged c9FTD mice exhibit reduced pyramidal neuron excitability in the dmPFC.
- Enhancing dmPFC activity rescues empathy loss in aged c9FTD mice.

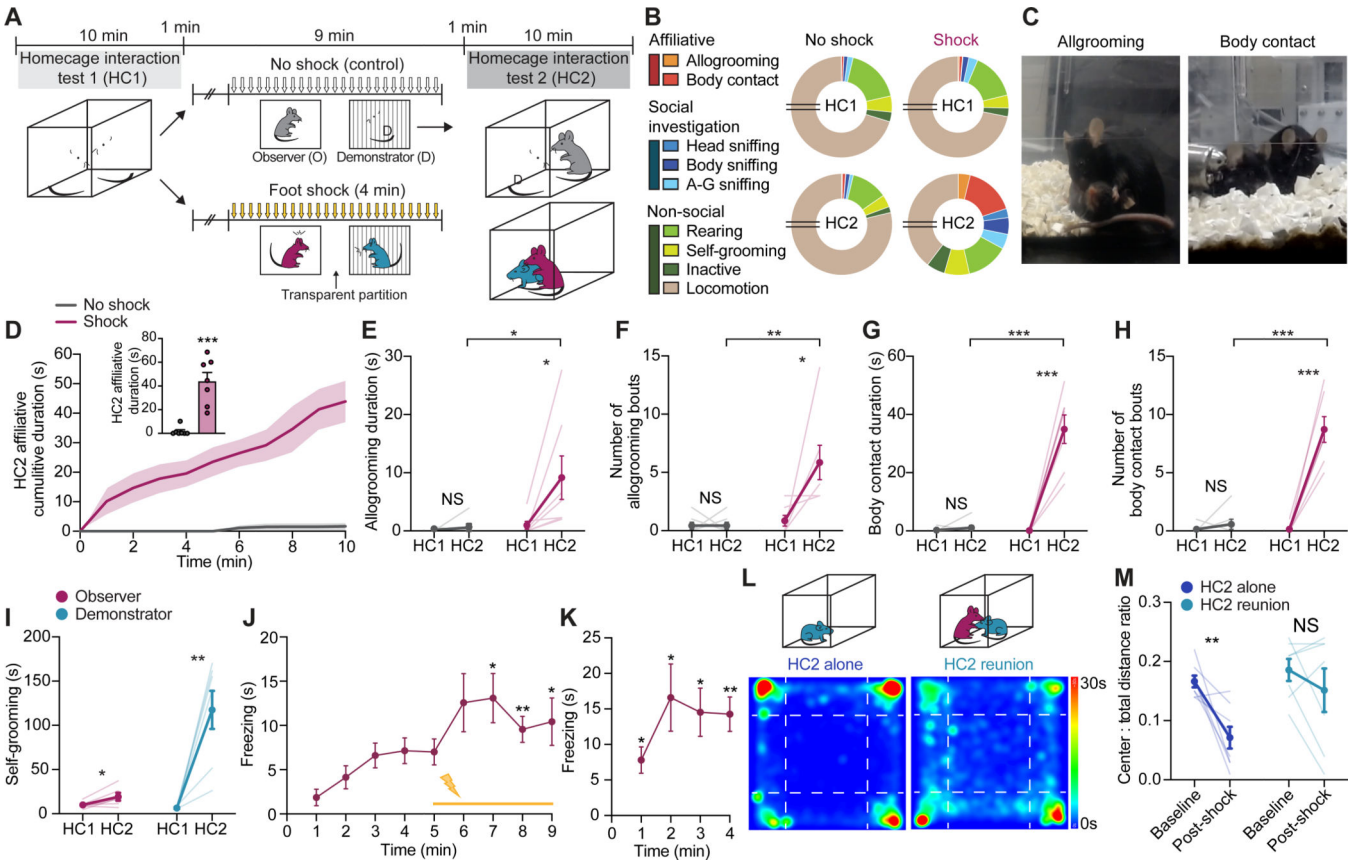

Figure 1. Other-directed consolation and emotional contagion in mice

(A) Schematic of DIA paradigm. O, Observer; D, Demonstrator.

(B) Proportions of time observers spent engaging in different behaviors in HC1 and HC2. A-G, anogenital. Breaks in pie charts indicate 6 minutes of locomotion.

(C) Representative images of allogrooming and body contact behaviors initiated by observers toward demonstrators in HC2.

(D) Cumulative duration of other-dir8ected affiliative behaviors by observers during HC2. Inset, summary of mean affiliative duration.

(E-H) Allogrooming duration (E) and number of bouts (F) and body contact duration (G) and number of bouts (H) by observers in HC1 and HC2.

(I) Self-grooming duration during HC1 and HC2 by observer and shocked demonstrator mice.

(J and K) Total time freezing exhibited by observers during conditioning (J) and retrieval (24 hours later) (K) of OFC.

(L and M) Representative heat maps (L) depicting cumulative time at different locations by demonstrators during a 30-minute open field test and quantification of center-to-total distance ratio (M) by demonstrators before (baseline) and after DIA (post-shock). Demonstrators either remained alone (left) or were reunited with observers (right) after foot-shocks.

Statistics: (D-I, M), two-tailed paired or unpaired Student's *t*-tests. (J and K), one-way repeated measures ANOVA with Dunnett's post-hoc tests comparing freezing to the first

minute of OFC baseline (no shock). *$P < .05$, **$P < .01$, ***$P < .001$. NS, not significant. See also Figure S1
and Video S1. In this and subsequent figures, data represents mean ± s.e.m. and statistical details are provided in Table S2.

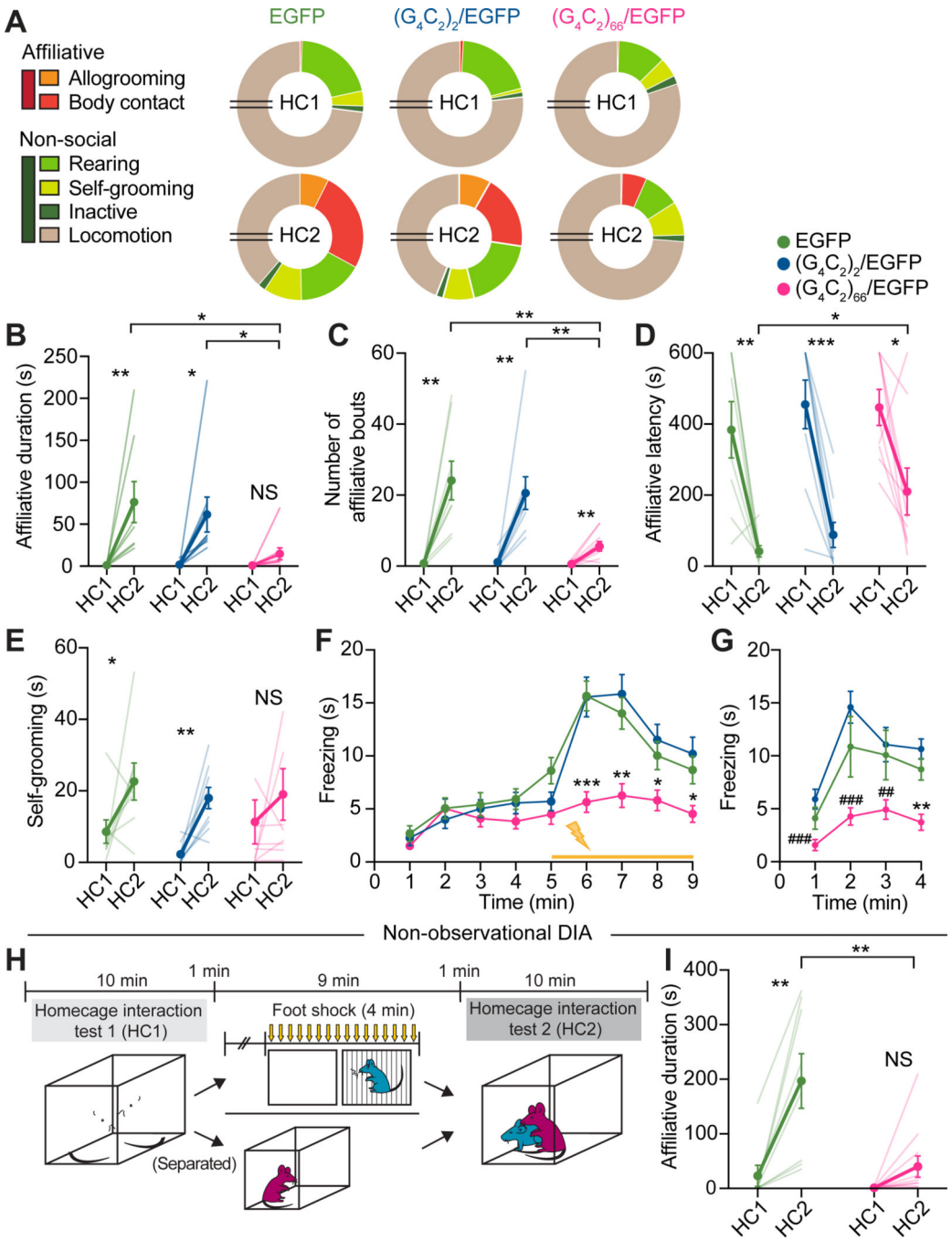

Figure 2. Impaired empathic function in aged $(G_4C_2)_{66}$/EGFP mice

(A) Proportions of time aged $(G_4C_2)_{66}$/EGFP, $(G_4C_2)_2$/EGFP, and EGFP observers spent engaging in different behaviors in DIA tests. Breaks in pie charts indicate 6 minutes of omitted locomotion and social investigation behaviors.

(B-D) Total duration (B), number of bouts (C), and latency (D) of affiliative behaviors by observers towards distressed demonstrators.

(E) Total self-grooming by observers during HC1 and HC2.

(F and G) Total freezing time by observers during conditioning (F) and 24-hour retrieval (G) of OFC.

(H) Schematic of non-observation DIA paradigm.

(I) Total duration of other-directed affiliative behaviors by aged $(G_4C_2)_{66}$/EGFP and EGFP observers during non-observational DIA tests.

Statistics: (B-E, I), two-tailed paired or unpaired Student's *t*-tests. (F and G), two-way repeated measures ANOVA with Bonferroni's post-hoc tests. $^{*}P < .05$, $^{**}P < .01$, $^{***}P < .001$ vs. both EGFP and $(G_4C_2)_2$/EGFP, where notations indicate the least significant *P* values of both comparisons. $^{\#\#}P < .01$, $^{\#\#\#}P < .001$ vs. $(G_4C_2)2$/EGFP. NS, not significant. See also Figure S2 and Video S1.

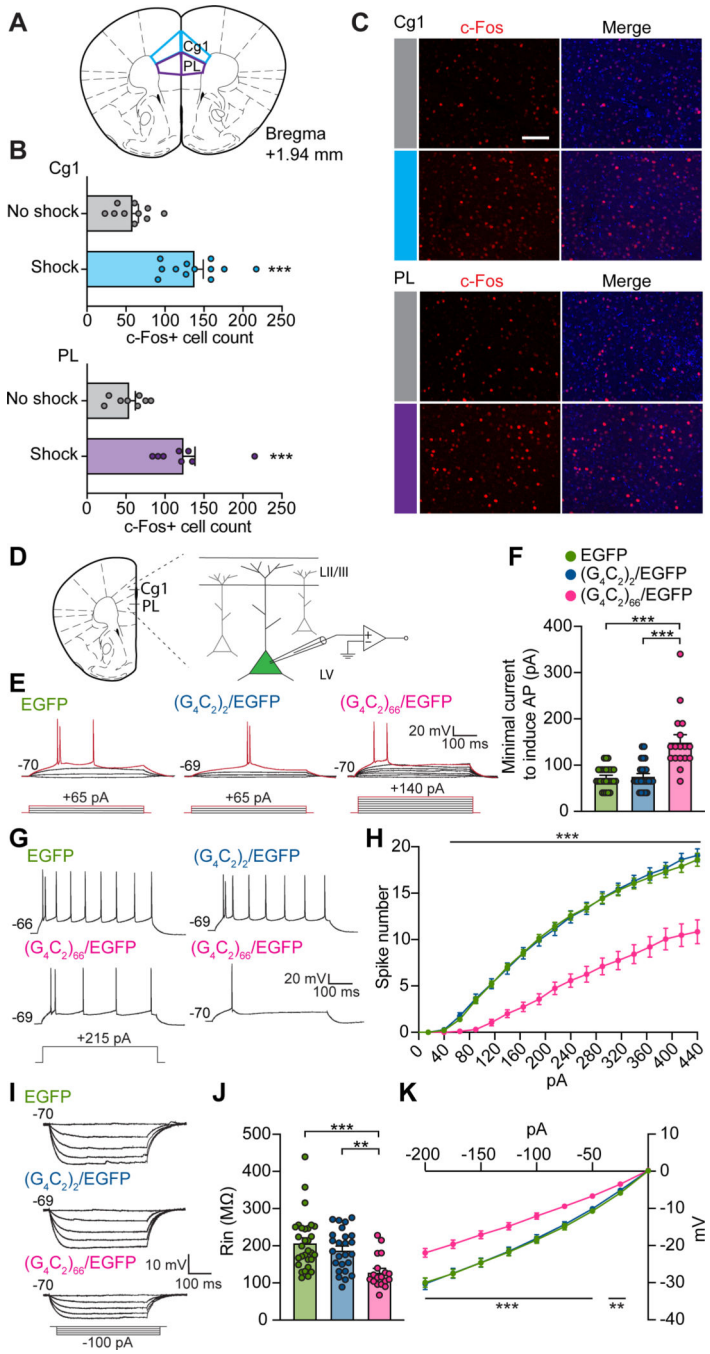

Figure 3. dmPFC hypoexcitability in aged $(G_4C_2)_{66}$/EGFP mice

(A) Schematic indicating Cg1 and PL subregions of the dmPFC sampled for c-Fos activation.

(B) Quantification of total c-Fos-positive cells from Cg1 (top) and PL (bottom) of observers exposed to shocked or non-shocked demonstrators during observational DIA test.

(C) Representative images of c-Fos-positive cells in Cg1 (top) and PL (bottom) of observers under no-shock and shock conditions. Nuclei were stained with DAPI (blue). Scale bar, 100 μm.

(D) Schematic of dmPFC recording configuration.
(E) Representative traces showing minimal current injections required to evoke APs (red traces) from $(G_4C_2)_{66}$/EGFP-, $(G_4C_2)2$/EGFP- and EGFP-expressing neurons in dmPFC.
(F) Summary of minimal currents required for AP firing from (E).
(G) Representative AP firing of mutant and control dmPFC neurons in response to a depolarizing step current injection (215 pA).
(H) Summary of AP numbers elicited by step current injections (500 ms, +25 pA steps).
(I) Representative traces of mutant and control dmPFC neurons in response to hyperpolarizing step current injections (500 ms, −25 pA steps).
(J and K) Summary of input resistance (J) and current-voltage relationship (K) from (I).
Statistics: (B), two-tailed unpaired Student's *t*-tests. (F and J), one-way ANOVA with Bonferroni's post-hoc tests. (H and K), two-way ANOVA with Bonferroni's post-hoc tests, where notations indicate the least significant *P* values of both comparisons. $^{**}P < .01$, $^{***}P < .001$. See also Table S1.

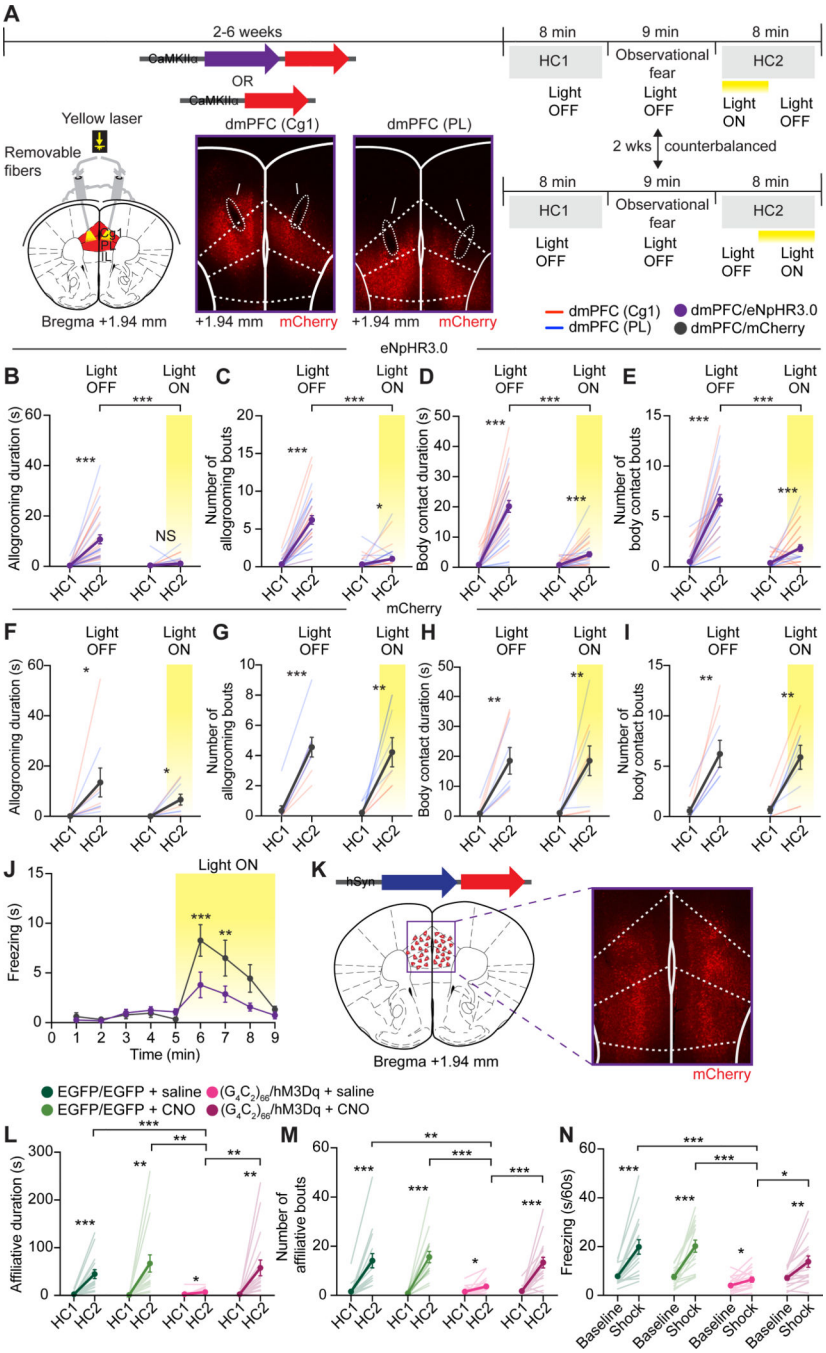

Figure 4. dmPFC-dependent mimic and rescue of FTD empathic deficits

(A) Schematic, representative viral injection sites and expression and fiber placements at two dmPFC targets, and timeline of *in vivo* optogenetic experiments. Arrows, optic fiber tracts.

(B-I) Allogrooming duration (B and F) and number of bouts (C and G) and body contact duration (D and H) and number of bouts (E and I) during HC1 and HC2 by eNPHR3.0 (B-E) and mCherry observers (F-I) in observational DIA tests. Data from Cg1-targeted mice

(dmPFC (Cg1); red lines) and PL-targeted mice (dmPFC (PL); blue lines) were combined to derive the means for dmPFC (dmPFC/eNpHR3.0 or dmPFC/mCherry).

(J) Freezing times by eNPHR3.0 and mCherry observers during OFC with photoinhibition.

(K) Representative AAV injection and expression in the dmPFC for *in vivo* chemogenetic experiments. Red triangles, injection sites.

(L-M) Affiliative duration (L) and number of bouts (M) by $(G_4C_2)_{66}$/hM3Dq or EGFP observers transduced with AAV2-hSyn-EGFP (EGFP/EGFP) towards demonstrators in saline or CNO conditions.

(N) Average freezing time during baseline or shock phase of OFC by observers after saline or CNO injections.

Statistics: (B-I, L-N), two-tailed paired or unpaired Student's *t*-tests. (J), two-way ANOVA with Bonferonni's post-hoc tests. $*P < .05$, $**P < .01$ $***P < .001$. See also Figures S3 and S4 and Video S2.

Key resources table

REAGENT or RESOURCE	SOURCE	IDENTIFIER
Antibodies		
Rabbit polyclonal anti-c-FOS	Synaptic Systems	Cat# 226003, RRID:AB_2231974
Rabbit monoclonal anti-NeuN	Millipore Sigma	Cat# MAB377, RRID:AB_2298772
Mouse anti-GFP	Novus	Cat# NB600–597, RRID:AB_10132090
Rabbit anti-$(GA)_8$	Covance	Custom
Rabbit anti-C9ORF72/C9RANT (poly-GR)	Millipore Sigma	Cat# ABN1361
Goat anti-mouse conjugated to Alexa 488	Invitrogen	Cat# A-21121, RRID:AB_2535764
Goat anti-rabbit conjugated to Alexa 555	Invitrogen	Cat# A-21428, RRID:AB_141784
Goat anti-rabbit conjugated to Alexa 586	Invitrogen	Cat# A-11011, RRID:AB_143157
Goat anti-rabbit conjugated to Alexa 488	Invitrogen	Cat# A-32731, RRID:AB_2633280
Bacterial and virus strains		
AAV2/9-$(G_4C_2)_{66}$	Chew et al., 2015	n/a
AAV2/9-$(G_4C_2)_2$	Chew et al., 2015	n/a
AAV9-EGFP	UMass Viral Vector Core	n/a
AAV2-hSyn-hM3D(Gq)-mCherry	B. Roth (unpublished data), Addgene	Cat# 50474, RRID:Addgene_50474
AAV2-hSyn-EGFP	B. Roth (unpublished data), Addgene	Cat# 50465, RRID:Addgene_50465
AAV2-hSyn-mCherry-WPRE	K. Deisseroth (unpublished data), Addgene	Cat# 114472 RRID:Addgene_114472
AAV5-CaMKIIα-eNpHR3.0-mCherry-WPRE	K. Deisseroth (unpublished data), UNC Vector Core	n/a
AAV5-CaMKIIα-mCherry-WPRE	K. Deisseroth (unpublished data), Addgene	Cat# 114469 RRID:Addgene_114469
Experimental models: Organisms/strains		
C57BL/6J mice	The Jackson Laboratory	Cat# 000664, RRID:IMSR_JAX:000664
Software and algorithms		
ANY-maze Version: 6.33	Stoelting Co.	https://www.any-maze.com/,RRID:SCR_014289
Clampex Version: 9.2	Molecular Devices	https://www.moleculardevices.com/products/axon-patch-clamp-system/acquisition-and-analysis-software/pclamp-software-suite,RRID:SCR_011323
Clampfit Version: 10.7.0.3	Molecular Devices	https://www.moleculardevices.com/products/axon-patch-clamp-system/acquisition-and-analysis-software/pclamp-software-suite,RRID:SCR_011323
Prism Version: 8.0	GraphPad Software	https://www.graphpad.com/scientific-software/prism/,RRID:SCR_002798
Fiji: 2.1.0	ImageJ	https://imagej.net/software/fiji/,RRID:SCR_002285
Olympus FV1000	Olympus	http://www.olympusconfocal.com/products/fv1000/fv1000software.html,RRID:SCR_014215

REAGENT or RESOURCE	SOURCE	IDENTIFIER
Zeiss Zen	Zeiss	https://www.zeiss.com/microscopy/us/products/microscope-software/zen.html,RRID:SCR_013672